# Interplay between Static and Dynamic Energy Transfer in Biofunctional Upconversion Nanoplatforms

**ARTICLE** *in* JOURNAL OF PHYSICAL CHEMISTRY LETTERS · JULY 2015

Impact Factor: 7.46 · DOI: 10.1021/acs.jpclett.5b00999



**11 AUTHORS**, INCLUDING:

Tom Gregorkiewicz

University of Amsterdam

**262** PUBLICATIONS **2,555** CITATIONS

SEE PROFILE

Xia Hong

Northeast Normal University

**28** PUBLICATIONS **680** CITATIONS

SEE PROFILE

M.C.G Aalders

University of Amsterdam

**125** PUBLICATIONS **2,432** CITATIONS

SEE PROFILE

Wybren J Buma

University of Amsterdam

**184** PUBLICATIONS **2,445** CITATIONS

SEE PROFILE

THE JOURNAL OF PHYSICAL CHEMISTRY Letters

Letter

pubs.acs.org/JPCL

# Interplay between Static and Dynamic Energy Transfer in Biofunctional Upconversion Nanoplatforms

Yadan Ding,[†,‡,#] Fei Wu,[‡,§] Youlin Zhang,[§] Xiaomin Liu,[§] Elinore M. L. D. de Jong,[⊥] Tom Gregorkiewicz,[⊥] Xia Hong,[†] Yichun Liu,*[,†] Maurice C. G. Aalders,[#] Wybren Jan Buma,[‡] and Hong Zhang*[,‡,§]

[†]Centre for Advanced Optoelectronic Functional Materials Research, Key Laboratory for UV Light-Emitting Materials and Technology of the Ministry of Education, Northeast Normal University, Changchun 130024, People's Republic of China

[‡]Van't Hoff Institute for Molecular Sciences and [⊥]van der Waals−Zeeman Institute, University of Amsterdam, Science Park 904, 1098 XH Amsterdam, The Netherlands

[§]State Key Laboratory of Luminescence and Applications, Changchun Institute of Optics, Fine Mechanics and Physics, Chinese Academy of Sciences, Changchun 130033, People's Republic of China

[#]Department of Biomedical Engineering and Physics, Academic Medical Center, University of Amsterdam, P.O. Box 22700, 1105 AZ Amsterdam, The Netherlands

Supporting Information

**ABSTRACT:** Clarification of the energy-transfer (ET) mechanism is of vital importance for constructing efficient upconversion nanoplatforms for biological/biomedical applications. Yet, most strategies of optimizing these nanoplatforms were casually based on a dynamic ET assumption. In this work, we have modeled quantitatively the shell-thickness-dependent interplay between dynamic and static ET in nanosystems and validated the model in a typical biofunctional upconversion nanoplatform composed of $NaYF_4$:Er, Yb/$NaYF_4$ upconversion nanoparticles (UCNPs), and energy-acceptor photosensitizing molecule Rose Bengal (RB). It was determined that with a proper thickness shell, the energy transferred via dynamic ET as well as static ET in this case could be significantly improved by ∼4 and ∼9 fold, respectively, compared with the total energy transferred from bare core UCNPs. Our results shall form the bedrock in designing highly efficient ET-based biofunctional nanoplatforms.

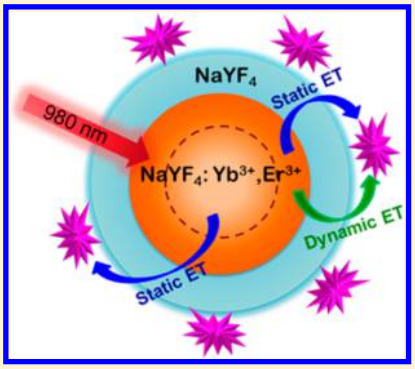


Lanthanide ion ($Ln^{3+}$)-doped upconversion nanoparticles (UCNPs) able to convert continuous-wave near-infrared (NIR) light into higher-energy and multicolor UV/visible light have been exploited intensively for various biological and biomedical applications.[1−3] They are more attractive than currently used materials in, for example, deep tissue penetration, and high detection sensitivity ascribed to the low photobleaching and absence of fluorescence interference of the background biological environment. Most of these applications are based on different energy-transfer (ET) mechanisms, for example, biosensing asks for high dynamic ET (Förster or fluorescence resonant energy transfer (FRET)) or static ET (inner filter effect or reabsorption), whereas photodynamic/thermal therapy requires high total ET including static and dynamic ET.[4−9]

In 2005, a homogeneous biosensor was reported using UCNPs as the energy donor.[10] In the presence of avidin, biotin conjugated $Na(Y_{1.5}Na_{0.5})F_6$:$Yb^{3+}$, $Er^{3+}$/$Tm^{3+}$ UCNPs (∼50 nm) and Au-biotin nanoparticles (the acceptor) were brought into close proximity through specific interaction between the avidin and biotin, and the upconversion luminescence was quenched via dynamic ET. On the basis of this effect, simple and sensitive detection of trace amounts of avidin was realized. Since then, many other nanomaterials and organic dyes, such as carbon nanoparticles, graphene oxide, and tetramethylrhodamine, have been introduced as energy acceptors into UCNP-based biochemical analysis of proteins, DNA, heavy metals, enzyme activities, and so forth.[1,11−14] The static ET process, where close proximity between the donor and acceptor is not required, was also utilized for the sensing of pH, $CO_2$, $Cr^{6+}$, and so forth.[15−18] In the meantime, other ET-based applications, for example, photodynamic therapy employing photosensitizing molecule conjugated upconversion nanoplatforms, were introduced as well.[18−20]

However, to bring these proof-of-concepts to application, there are huge challenges. One crucial issue is that the ET needs to be largely enhanced because the state-of-the-art upconversion efficiency is below 1% for nanomaterials under a clinically acceptable excitation level.[21] Until now, the picture of the ET mechanism has not been well explored, as witnessed by

**Received:** May 14, 2015
**Accepted:** June 15, 2015
**Published:** June 15, 2015





DOI: 10.1021/acs.jpclett.5b00999
J. Phys. Chem. Lett. 2015, 6, 2518−2523

the fact that most relevant ET has been treated as dynamic in nature. The distance dependence of FRET was generally taken as the basis for optimizing the biofunctional nanoplatforms that led to the popular approach (shortening the distance between the UCNPs and the energy acceptors), and naturally, a bare-core structure was dominantly adopted.[1,22−26] Recently, there were some indications that ET mechanisms other than FRET might not be neglected between a closely located donor and acceptor.[27−31] For example, reabsorption was shown to be the primary reason for the luminescence quenching of $NaYF_4$:$Yb^{3+}$, $Er^{3+}$ UCNPs (~23.5 nm, the donor) encapsulated by an amphiphilic polymer shell containing photoresponsive diarylethene chromophores (the acceptor).[30] Similar phenomena were also reported when CdSe quantum dots were used as the energy acceptor in the solid state.[31]

Therefore, to have a quantitative picture of the roles that the static and dynamic ET play in the biofunctional nanoplatforms is very urgent for constructing efficient ET structures and of key importance for bioapplications of these very promising nanoplatforms. In this work, we separate quantitatively the dynamic and static ET and their weights in ET from theoretical modeling and corresponding spectroscopic experiments and validate the picture using a typical biofunctional nanoplatform. In a dynamic ET process, energy is transferred to the acceptor nonradiatively from the excited state of the donor, providing an additional nonradiative relaxation channel for the donor emissive energy level, resulting in a shortened lifetime of the donor emission. Whereas in the static ET process the energy is transferred to the acceptor after the radiative relaxation process of the donor, the temporal behavior of the donor emission is thus not affected.

Considering the spatial distribution of the emitting centers and the relatively large size of UCNPs (compared with typical Förster distance of less than 10 nm), only the emitting centers close to the surface-bound acceptors can transfer energy effectively via dynamic ET. Therefore, we can reasonably divide the doped area of UCNPs into two parts; one is the outer layer where the emitting centers participate in both dynamic and static ET and thus have fast emission kinetics, and the other one is the central area where the emitting centers are farther away from surface-bound acceptors and thus not involved in dynamic ET, retaining slow emission kinetics.

An important biofunctional upconversion nanoplatform is taken as the sample system in this case, which is composed of core−shell $NaYF_4$:$Yb^{3+}$, $Er^{3+}$/$NaYF_4$ and a covalently conjugated photosensitizing molecule, Rose Bengal (RB) (Figure 1A), and the absorption and emission spectra of $NaYF_4$:$Yb^{3+}$, $Er^{3+}$ UCNPs and RB are depicted in Figure 1B. Obviously, NIR 980 nm excitation, once upconverted in UCNPs to ~540 nm, can be transferred to RB via static and/or dynamic ET mechanisms due to the large overlap of the 540 nm (green) emission band and the absorption spectrum of RB, whereas the upconversion emission band at ~650 nm (red) does not participate in the ET because it does not overlap spectrally with RB absorption.

Assuming that the time evolution of the green emission of UCNPs without the acceptor RB under NIR light excitation is described with a biexponential function, that is

$$I(t)_{\mathrm{D}} = A_1 \exp\left(-\frac{t}{\tau_{\mathrm{rise}}}\right) + A_2 \exp\left(-\frac{t}{\tau_2}\right) \quad (1)$$

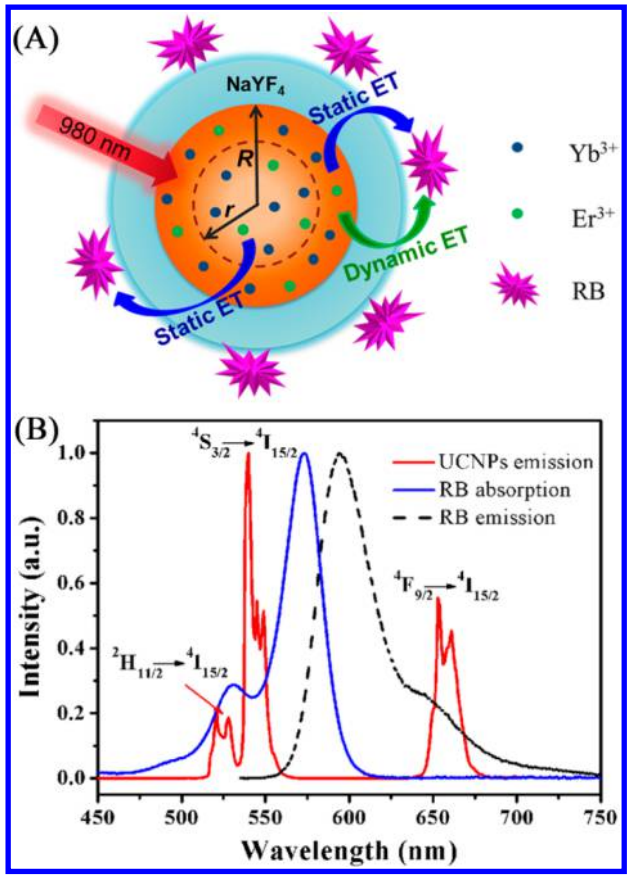


**Figure 1.** (A) ET model from $Er^{3+}$ in core−shell $NaYF_4$:$Yb^{3+}$, $Er^{3+}$/$NaYF_4$ UCNPs to surface-bound acceptor RB. *R* denotes the radius of the $NaYF_4$:$Yb^{3+}$, $Er^{3+}$ core, and *r* denotes the radius of its central area where $Er^{3+}$ participates solely in the static ET process. (B) The absorption and emission spectra of UCNPs and RB.

where $\tau_2$ is the decay time constant. When bounded on the surface of the UCNPs, RB can be excited (1) via static ET, that is, absorption of the 540 nm emission of UCNPs, and (2) via dynamic ET. Therefore, the time evolution of the 540 nm upconversion emission can be approximately described as

$$I(t)_{\mathrm{D-A}} = A_1 \exp\left(-\frac{t}{\tau_{\mathrm{rise,RB}}}\right) + A_2 \exp\left(-\frac{t}{\tau_2}\right) + A_3 \exp\left(-\frac{t}{\tau_3}\right) \quad (2)$$

Here, the additional short decay component with time constant $\tau_3$ represents emitters in the outer layer of UCNPs that experience dynamic ET. $\tau_{\mathrm{rise,RB}}$ represents the rise time constant when RB exists.

Because the lifetime of upconversion luminescence (micro- to milliseconds) is much longer than that of RB (pico- to nanoseconds), the time evolution of RB emission shall mimic that of upconversion luminescence when they are excited via ET from UCNPs regardless of being dynamic or static.[32−34] Therefore, the temporal behavior of RB emission can also be described with a triexponential function with the time constants of eq 2



DOI: 10.1021/acs.jpclett.5b00999
J. Phys. Chem. Lett. 2015, 6, 2518−2523

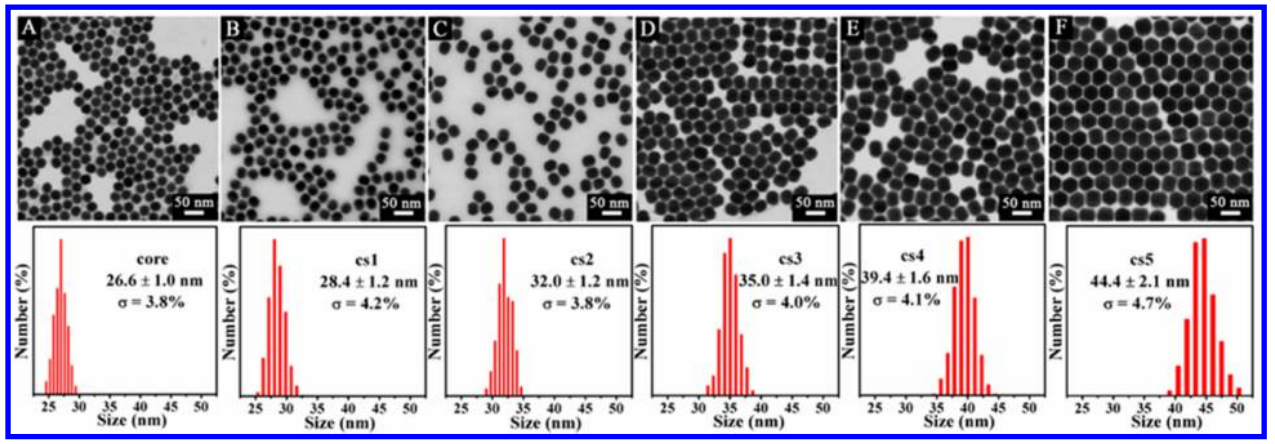


**Figure 2.** Bright-field SEM images and size distribution of $NaYF_4$:$Yb^{3+}$, $Er^{3+}$ core (A) and $NaYF_4$:$Yb^{3+}$, $Er^{3+}$/$NaYF_4$ core−shell UCNPs (B−F corresponds to cs1 to cs5, respectively). The size distribution was given by averaging the diameter ± standard deviation (more than 300 nanoparticles were counted).

$$I'(t)_{\mathrm{A-D}} = A_1' \exp\left(-\frac{t}{\tau_{\mathrm{rise,RB}}}\right) + A_2' \exp\left(-\frac{t}{\tau_2}\right) + A_3' \exp\left(\frac{t}{\tau_3}\right) \quad (3)$$

The amplitude ratio $A_2/A_3$ of the slow to the fast decay components in eq 2 represents also the ratio of the numbers of emitting centers in the central area to the outer layer of UCNPs. The amplitude ratio $A_2'/A_3'$ provides more important information about acceptor excitation. It is known that dynamic ET efficiency depends on the donor−acceptor distance with an inverse $n$th power law ($n > 3$),[35−38] while the static ET rate drops off according to the inverse square law in relation with the absorption cross section of the acceptor; static ET is thus less sensitive to the separation distance. On the basis of this, we can separate the contributions of dynamic ET and static ET of the emitters in the outer layer of UCNPs by rewriting eq 3 to

$$I'(t)_{\mathrm{A-D}} = A_1' \exp\left(-\frac{t}{\tau_{\mathrm{rise,RB}}}\right) + A_2' \exp\left(-\frac{t}{\tau_2}\right) + A_3'' \exp\left(-\frac{t}{\tau_3}\right) + B \exp\left(-\frac{t}{\tau_3}\right) \quad (4)$$

where $A_3' = A_3'' + B$, $A_3''$ denotes the contribution of static ET, and $B$ denotes the contribution of dynamic ET. Because

$$\frac{A_2'}{A_3''} = \frac{A_2}{A_3} \quad (5)$$

the ratio between the contributions of dynamic and static ET from the emitting centers in the outer layer area is thus

$$\frac{D}{S} = \frac{B}{A_3''} = \frac{A_2 A_3'}{A_2' A_3} - 1 \quad (6)$$

To validate this model, we have varied the shell thickness of the UCNPs and monitored the time evolution of the upconversion emission and RB emission. $NaYF_4$:$Yb^{3+}$, $Er^{3+}$ core, and $NaYF_4$:$Yb^{3+}$, $Er^{3+}$/$NaYF_4$ core−shell UCNPs with increasing shell thickness (from cs1 to cs5) were synthesized following a self-focusing strategy utilizing Ostwald ripening dynamics.[39] XRD patterns are shown in Figure S1 in the Supporting Information (SI), confirming the hexagonal phase of all of the samples. Figure 2 illustrates the high monodispersity of the samples.

Steady-state emission spectra of the six samples were recorded, as shown in Figure 3. Despite the continuous

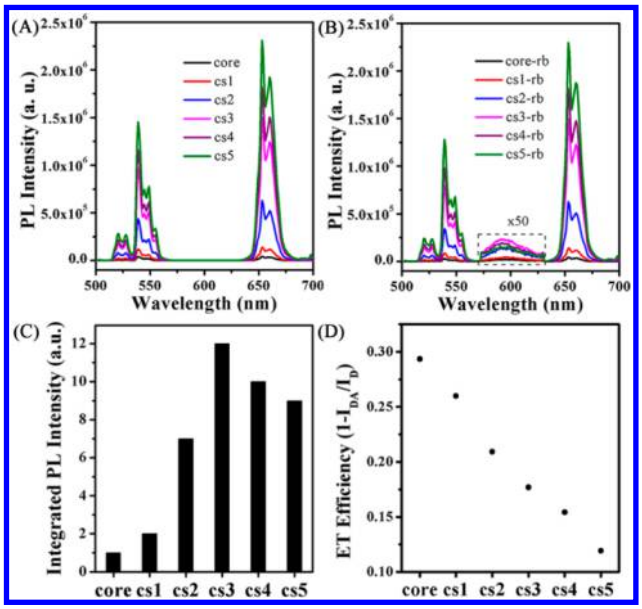


**Figure 3.** Emission spectra of UCNPs (A) and UCNP-RB samples (B) under 980 nm excitation. The RB emission band peaking at ∼590 nm in (B) is magnified by 50 times. (C) The integrated intensity of the RB emission band in (B). (D) ET efficiency of the six UCNP-RB samples. The emission spectra were normalized at 650 nm for each sample before calculation.

increase of the green and red upconversion emission and monotonous decrease of ET efficiency under 980 nm excitation, the RB emission peaking at ∼590 nm demonstrates that a maximal intensity was observed for sample cs3.

The time evolution of the green upconversion and RB emission of the six samples is shown in Figure 4. All of the curves could be well fitted by eqs 1 and 2, validating the theoretical model. Relevant parameters are listed in Tables 1 and S1 (in the SI). It can be seen that the decay of the 540 nm emission becomes longer when the shell gets thicker, consistent with the effective deactivation of surface-related nonradiative


DOI: 10.1021/acs.jpclett.5b00999
J. Phys. Chem. Lett. 2015, 6, 2518−2523

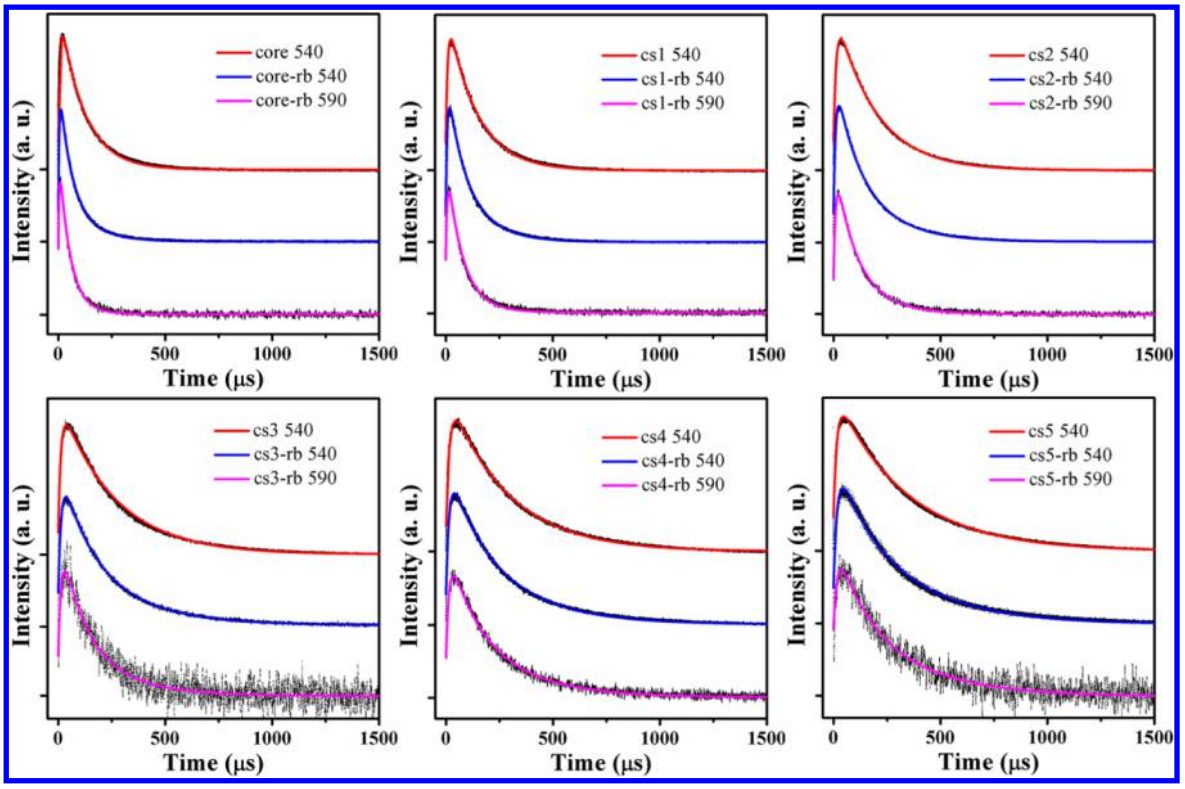


**Figure 4.** Time behavior of upconversion luminescence of UCNPs (red curves) and UCNP-RB (blue curves) at 540 nm and RB emission of UCNP-RB at 590 nm (magenta curves) under 980 nm excitation. The raw data are presented with black scatter, and the fitted results are shown with colored solid curves.

**Table 1. Fitted Time Constants for UCNP-RB Samples and the Amplitude Ratio for 540 ($A_2/A_3$) and 590 nm ($A_2'/A_3'$)**

| | core | cs1 | cs2 | cs3 | cs4 | cs5 |
|---|---|---|---|---|---|---|
| $\tau_{rise,RB}/\mu s$ | 4.50 | 6.62 | 9.31 | 13.88 | 14.16 | 16.66 |
| $\tau_2/\mu s$ | 113.71 | 136.50 | 187.08 | 255.59 | 276.50 | 327.39 |
| $\tau_3/\mu s$ | 50.29 | 69.84 | 91.97 | 113.32 | 122.82 | 130.54 |
| $A_2/A_3$ | 0.61 | 1.05 | 1.40 | 1.90 | 3.03 | 3.21 |
| $A_2'/A_3'$ | 0.06 | 0.11 | 0.31 | 0.46 | 1.31 | 1.56 |

relaxation processes, and the emission kinetics is always faster in UCNP-RB samples than that in the corresponding UCNPs, whereas for 650 nm emission, the temporal behavior of UCNPs and corresponding UCNP-RB are almost the same as shown in Figure S2 and Table S2 (SI). It confirms the occurrence of dynamic ET in the green spectral region from UCNPs to RB molecules.

The amplitude ratio $A_2/A_3$ of the slow to the fast components of 540 nm emission in Table 1 gets larger with an increase of the shell thickness, indicating that more emitting centers are out of the dynamic ET interaction distance. It is consistent with the distance increase between the doped area of UCNPs and RB molecules. Assuming that the emitting centers are distributed evenly in the core of UCNPs, the two areas can be calculated from $A_2/A_3$, and the dynamic ET interaction distance was found to be shell-thickness-dependent (see eq S1 and the relevant analysis in the SI). For UCNPs with the thickest shell, the upconversion luminescence quantum efficiency is enhanced by ~36-fold, and accordingly, the Förster distance is about 1.8 times that of the bare core. Therefore, with this $NaYF_4$ shell on the surface of $NaYF_4$:$Yb^{3+}$, $Er^{3+}$ UCNPs, the donor−acceptor distance is increased, disabling dynamic ET; in the meantime, however, the dynamic ET interaction distance is increased due to the enhancement of upconversion luminescence, which is beneficial for dynamic ET performance. Therefore, an optimal shell thickness exists for dynamic ET as well.

Shell-thickness-dependent interplay between dynamic and static ET could be obtained from eqs 6 and S2 (SI), and the results are shown in Table 2. The decrease of $D/S$ from ~10 to ~1 means for the emitting centers in the outer layer of UCNPs, a dynamic ET process plays an important role, but it becomes less effective when the donor−acceptor distance is increased. It is also seen that with an increase of the shell thickness from 0 to 8.9 nm, the contribution of dynamic ET to the total transferred energy decreases from ~80 to ~7%, and in the meantime, static ET contributes from ~20 to ~93%. For bare core and thin-shell UCNPs, dynamic ET is the main ET mechanism. When the shell thickness increases to more than 6 nm, although dynamic ET can still occur for the emitting centers closest to the surface, it is less effective because most of the emitting centers are nearly out of dynamic ET interaction distance. The most

**Table 2. Shell Thicknesses of the Six UCNP Samples and the Dynamic and Static ET Components for RB Excitation[a]**

| | core | cs1 | cs2 | cs3 | cs4 | cs5 |
|---|---|---|---|---|---|---|
| shell thickness/nm | 0 | 0.9 | 2.7 | 4.2 | 6.4 | 8.9 |
| $D/S$ | 10.02 | 8.30 | 3.60 | 3.10 | 1.32 | 1.05 |
| $I_{dynamic}/I_{total}$ | 0.80 | 0.71 | 0.45 | 0.32 | 0.10 | 0.07 |
| $I_{dynamic}/I_0$ | 0.80 | 1.42 | 3.15 | 3.84 | 1.00 | 0.63 |
| $I_{static}/I_0$ | 0.20 | 0.58 | 3.85 | 8.16 | 9.00 | 8.37 |

[a] $I_0$ denotes the total emission of RB from the core-RB sample.



DOI: 10.1021/acs.jpclett.5b00999
J. Phys. Chem. Lett. 2015, 6, 2518−2523

efficient dynamic or static ET occurs in the core−shell sample with more or less the same shell thickness where the most efficient ET (dynamic plus static ET) occurs.

In conclusion, aiming at optimizing the biofunctional upconversion nanoplatforms, the shell role in the interplay between static and dynamic ET mechanisms has been elucidated for the first time for upconversion nanosystems. The ET process was modeled and experimentally validated on a typical biofunctional upconversion nanoplatform. From the obtained relation, it was determined that although the contribution of the dynamic part in ET decreases when the shell gets thicker, it reaches a maximum with a shell thickness of ∼4 nm. On the contrary, the contribution of static ET increases when the shell gets thicker and reaches a maximum with a similar shell thickness. In a word, optimization of static ET, as well as dynamic ET, in biofunctional nanoplatforms can be achieved by coating a proper shell. This work is significant in optimization of upconversion nanoplatforms applied in, but not limited to, bioassays and photodynamic/thermal therapies.

## ■ ASSOCIATED CONTENT

### Supporting Information

Experimental details. Data analysis. XRD patterns of UCNPs. Time behavior of upconversion luminescence at 650 nm. The fitting results. The Supporting Information is available free of charge on the ACS Publications website at DOI: 10.1021/acs.jpclett.5b00999.

## ■ AUTHOR INFORMATION

### Corresponding Authors

*E-mail: h.zhang@uva.nl (H.Z.).
*E-mail: ycliu@nenu.edu.cn (Y.L.).

### Notes

The authors declare no competing financial interest.

## ■ ACKNOWLEDGMENTS

This work was supported by the Innovation Program (IOP) of The Netherlands, Innovation project of the State Key Laboratory of Luminescence and Applications, Natural Science Foundation of China (No. 11174277, 11474278, 51272040), the Program for New Century Excellent Talents in University of Ministry of Education of China, the Joint research program between KNAW of The Netherlands and CAS of China, the John van Geuns Foundation, and the Dutch Technology Foundation STW, which is part of The Netherlands Organisation for Scientific Research (NWO) and which is partly funded by the Ministry of Economic Affairs. Y.D. and H.Z. are grateful to Dr. Yingkai Huang (van der Waals−Zeeman Institute, University of Amsterdam) for XRD measurements, and to Dr. Andries Lof (AMOLF) for SEM measurements.

## ■ REFERENCES

(1) Chen, G.; Qju, H.; Prasad, P. N.; Chen, X. Upconversion Nanoparticles: Design, Nanochemistry, and Applications in Theranostics. *Chem. Rev.* **2014**, *114*, 5161−5214.
(2) Idris, N. M.; Jayakumar, M. K.; Bansal, A.; Zhang, Y. Upconversion Nanoparticles as Versatile Light Nanotransducers for Photoactivation Applications. *Chem. Soc. Rev.* **2015**, *44*, 1449−1478.
(3) Yang, D.; Ma, P.; Hou, Z.; Cheng, Z.; Li, C.; Lin, J. Current Advances in Lanthanide Ion (Ln)-Based Upconversion Nanomaterials for Drug Delivery. *Chem. Soc. Rev.* **2014**, *44*, 1416−1448.
(4) Idris, N. M.; Gnanasammandhan, M. K.; Zhang, J.; Ho, P. C.; Mahendran, R.; Zhang, Y. In Vivo Photodynamic Therapy Using Upconversion Nanoparticles as Remote-Controlled Nanotransducers. *Nat. Med.* **2012**, *18*, 1580−1585.
(5) Wang, P.; Joshi, P.; Alazemi, A.; Zhang, P. Upconversion Nanoparticle-Based Ligase-Assisted Method for Specific and Sensitive Detection of T790M Mutation in Epidermal Growth Factor Receptor. *Biosens. Bioelectron.* **2014**, *62*, 120−126.
(6) Chen, H.; Yuan, F.; Wang, S.; Xu, J.; Zhang, Y.; Wang, L. Aptamer-Based Sensing for Thrombin in Red Region via Fluorescence Resonant Energy Transfer between $NaYF_4$:Yb,Er Upconversion Nanoparticles and Gold Nanorods. *Biosens. Bioelectron.* **2013**, *48*, 19−25.
(7) Qiao, X.; Zhou, J.; Xiao, J.; Wang, Y.; Sun, L.; Yan, C. Triple-Functional Core−Shell Structured Upconversion Luminescent Nanoparticles Covalently Grafted with Photosensitizer for Luminescent, Magnetic Resonance Imaging and Photodynamic Therapy in Vitro. *Nanoscale* **2012**, *4*, 4611−4623.
(8) Lucky, S. S.; Idris, N.; Muhammad, L. Z.; Huang, K.; Soo, K. C.; Zhang, Y. Titania Coated Upconversion Nanoparticles for Near-Infrared Light Triggered Photodynamic Therapy. *ACS Nano* **2015**, *9*, 191−205.
(9) Sun, L.-N.; Peng, H.; Stich, M. I. J.; Achatz, D.; Wolfbeis, O. S. pH Sensor Based on Upconverting Luminescent Lanthanide Nanorods. *Chem. Commun.* **2009**, *33*, 5000−5002.
(10) Wang, L.; Yan, R.; Huo, Z.; Wang, L.; Zeng, J.; Bao, J.; Wang, X.; Peng, Q.; Li, Y. Fluorescence Resonant Energy Transfer Biosensor Based on Upconversion-Luminescent Nanoparticles. *Angew. Chem., Int. Ed.* **2005**, *44*, 6054−6057.
(11) Deng, R.; Xie, X.; Vendrell, M.; Chang, Y. T.; Liu, X. Intracellular Glutathione Detection Using $MnO_2$-Nanosheet-Modified Upconversion Nanoparticles. *J. Am. Chem. Soc.* **2011**, *133*, 20168−20171.
(12) Liu, C.; Chang, L.; Wang, H.; Bai, J.; Ren, W.; Li, Z. Upconversion Nanophosphor: An Efficient Phosphopeptides-Recognizing Matrix and Luminescence Resonance Energy Transfer Donor for Robust Detection of Protein Kinase Activity. *Anal. Chem.* **2014**, *86*, 6095−6102.
(13) Liu, J.; Cheng, J.; Zhang, Y. Upconversion Nanoparticle Based LRET System for Sensitive Detection of MRSA DNA Sequence. *Biosens. Bioelectron.* **2013**, *43*, 252−256.
(14) Xu, S.; Xu, S.; Zhu, Y.; Xu, W.; Zhou, P.; Zhou, C.; Dong, B.; Song, H. A Novel Upconversion, Fluorescence Resonance Energy Transfer Biosensor (FRET) for Sensitive Detection of Lead Ions in Human Serum. *Nanoscale* **2014**, *6*, 12573−12579.
(15) Xie, L.; Qin, Y.; Chen, H. Polymeric Optodes Based on Upconverting Nanorods for Fluorescent Measurements of pH and Metal Ions in Blood Samples. *Anal. Chem.* **2012**, *84*, 1969−1974.
(16) Ali, R.; Saleh, S. M.; Meier, R. J.; Azab, H. A.; Abdelgawad, I. I.; Wolfbeis, O. S. Upconverting Nanoparticle Based Optical Sensor for Carbon Dioxide. *Sens. Actuators, B* **2010**, *150*, 126−131.
(17) Chen, H.; Ren, J. Sensitive Determination of Chromium (VI) Based on the Inner Filter Effect of Upconversion Luminescent Nanoparticles ($NaYF_4$:$Yb^{3+}$, $Er^{3+}$). *Talanta* **2012**, *99*, 404−408.
(18) Zhou, J.; Liu, Q.; Feng, W.; Sun, Y.; Li, F. Upconversion Luminescent Materials: Advances and Applications. *Chem. Rev.* **2015**, *115*, 395−465.
(19) Liu, K.; Liu, X.; Zeng, Q.; Zhang, Y.; Tu, L.; Liu, T.; Kong, X.; Wang, Y.; Cao, F.; Lambrechts, S. A. G.; et al. Covalently Assembled NIR Nanoplatform for Simultaneous Fluorescence Imaging and Photodynamic Therapy of Cancer Cells. *ACS Nano* **2012**, *6*, 4054−4062.
(20) Wang, C.; Tao, H.; Cheng, L.; Liu, Z. Near-Infrared Light Induced in Vivo Photodynamic Therapy of Cancer Based on Upconversion Nanoparticles. *Biomaterials* **2011**, *32*, 6145−6154.
(21) Boyer, J. C.; van Veggel, F. C. J. M. Absolute Quantum Yield Measurements of Colloidal $NaYF_4$: $Er^{3+}$, $Yb^{3+}$ Upconverting Nanoparticles. *Nanoscale* **2010**, *2*, 1417−1419.


DOI: 10.1021/acs.jpclett.5b00999
*J. Phys. Chem. Lett.* 2015, 6, 2518−2523

(22) Yuan, Y.; Liu, Z. An Effective Approach to Enhanced Energy-Transfer Efficiency from Up-Converting Phosphors and Increased Assay Sensitivity. *Chem. Commun.* **2012**, *48*, 7510−7512.
(23) Wang, M.; Chen, Z.; Zheng, W.; Zhu, H.; Lu, S.; Ma, E.; Tu, D.; Zhou, S.; Huang, M.; Chen, X. Lanthanide-Doped Upconversion Nanoparticles Electrostatically Coupled with Photosensitizers for Near-Infrared-Triggered Photodynamic Therapy. *Nanoscale* **2014**, *6*, 8274−8282.
(24) Hu, X.; Wei, T.; Wang, J.; Liu, Z.-E.; Li, X.; Zhang, B.; Li, Z.; Li, L.; Yuan, Q. Near-Infrared-Light Mediated Ratiometric Luminescent Sensor for Multimode Visualized Assays of Explosives. *Anal. Chem.* **2014**, *86*, 10484−10491.
(25) Tian, G.; Ren, W.; Yan, L.; Jian, S.; Gu, Z.; Zhou, L.; Jin, S.; Yin, W.; Li, S.; Zhao, Y. Red-Emitting Upconverting Nanoparticles for Photodynamic Therapy in Cancer Cells under Near-Infrared Excitation. *Small* **2013**, *9*, 1929−1938.
(26) Hwang, S. H.; Im, S. G.; Sung, H.; Hah, S. S.; Cong, V. T.; Lee, D. H.; Son, S. J.; Oh, H. B. Upconversion Nanoparticle-Based Förster Resonance Energy Transfer for Detecting the IS6110 Sequence of Mycobacterium Tuberculosis Complex in Sputum. *Biosens. Bioelectron.* **2014**, *53*, 112−116.
(27) Chen, R.; Ta, V. D.; Xiao, F.; Zhang, Q. Y.; Sun, H. D. Multicolor Hybrid Upconversion Nanoparticles and Their Improved Performance as Luminescence Temperature Sensors Due to Energy Transfer. *Small* **2013**, *9*, 1052−1057.
(28) Riuttamaki, T.; Hyppanen, I.; Kankare, J.; Soukka, T. Decrease in Luminescence Lifetime Indicating Nonradiative Energy Transfer from Upconverting Phosphors to Fluorescent Acceptors in Aqueous Suspensions. *J. Phys. Chem. C* **2011**, *115*, 17736−17742.
(29) Wu, T.; Wilson, D.; Branda, N. R. Fluorescent Quenching of Lanthanide-Doped Upconverting Nanoparticles by Photoresponsive Polymer Shells. *Chem. Mater.* **2014**, *26*, 4313−4320.
(30) Wu, T.; Boyer, J. C.; Barker, M.; Wilson, D.; Branda, N. R. A "Plug-and-Play" Method to Prepare Water-Soluble Photoresponsive Encapsulated Upconverting Nanoparticles Containing Hydrophobic Molecular Switches. *Chem. Mater.* **2013**, *25*, 2495−2502.
(31) Bednarkiewicz, A.; Nyk, M.; Samoc, M.; Strek, W. Up-Conversion FRET from $Er^{3+}/Yb^{3+}$:$NaYF_4$ Nanophosphor to CdSe Quantum Dots. *J. Phys. Chem. C* **2010**, *114*, 17535−17541.
(32) Cramer, L. E.; Spears, K. G. Hydrogen-Bond Strengths from Solvent-Dependent Lifetimes of Rose-Bengal Dye. *J. Am. Chem. Soc.* **1978**, *100*, 221−227.
(33) Ju, Q.; Tu, D.; Liu, Y.; Li, R.; Zhu, H.; Chen, J.; Chen, Z.; Huang, M.; Chen, X. Amine-Functionalized Lanthanide-Doped $KGdF_4$ Nanocrystals as Potential Optical/Magnetic Multimodal Bioprobes. *J. Am. Chem. Soc.* **2012**, *134*, 1323−1330.
(34) Wang, Y.; Liu, K.; Liu, X.; Dohnalova, K.; Gregorkiewicz, T.; Kong, X.; Aalders, M. C. G.; Buma, W. J.; Zhang, H. Critical Shell Thickness of Core/Shell Upconversion Luminescence Nanoplatform for FRET Application. *J. Phys. Chem. Lett.* **2011**, *2*, 2083−2088.
(35) Sen, T.; Sadhu, S.; Patra, A. Surface Energy Transfer from Rhodamine 6G to Gold Nanoparticles: A Spectroscopic Ruler. *Appl. Phys. Lett.* **2007**, *91*, 043104.
(36) Yun, C. S.; Javier, A.; Jennings, T.; Fisher, M.; Hira, S.; Peterson, S.; Hopkins, B.; Reich, N. O.; Strouse, G. F. Nanometal Surface Energy Transfer in Optical Rulers, Breaking the FRET Barrier. *J. Am. Chem. Soc.* **2005**, *127*, 3115−3119.
(37) Stryer, L.; Haugland, R. P. Energy Transfer: A Spectroscopic Ruler. *Proc. Natl. Acad. Sci. U.S.A.* **1967**, *58*, 719−726.
(38) Li, M.; Cushing, S. K.; Wang, Q.; Shi, X.; Hornak, L. A.; Hong, Z.; Wu, N. Size-Dependent Energy Transfer between CdSe/ZnS Quantum Dots and Gold Nanoparticles. *J. Phys. Chem. Lett.* **2011**, *2*, 2125−2129.
(39) Johnson, N. J. J.; Korinek, A.; Dong, C.; van Veggel, F. C. J. M. Self-Focusing by Ostwald Ripening: A Strategy for Layer-by-Layer Epitaxial Growth on Upconverting Nanocrystals. *J. Am. Chem. Soc.* **2012**, *134*, 11068−11071.


DOI: 10.1021/acs.jpclett.5b00999
*J. Phys. Chem. Lett.* 2015, 6, 2518−2523